

pubs.acs.org/cm Article

Ion Coordination and Chelation in a Glycolated Polymer Semiconductor: Molecular Dynamics and X-ray Fluorescence Study

Micaela Matta,* Ruiheng Wu, Bryan D. Paulsen, Anthony J. Petty, II, Rajendar Sheelamanthula, Iain McCulloch, George C. Schatz, and Jonathan Rivnay



Cite This: Chem. Mater. 2020, 32, 7301-7308



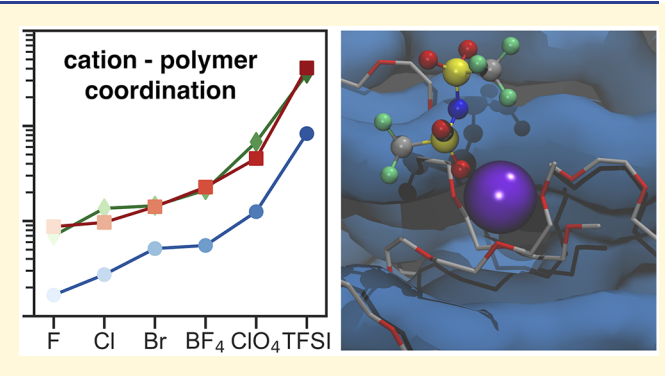
ACCESS

Metrics & More

Article Recommendations

Supporting Information

ABSTRACT: Polythiophenes bearing glycolated side chains have rapidly surged as the highest performing materials for organic electrochemical transistors (OECTs) because of their ability to conjugate volumetric ion penetration with high hole mobility and charge density. Among them, p(g2T-TT) has one of the highest figures of merit. Our work provides an atomistic picture of the p(g2T-TT)—electrolyte interface in the "off" state of an OECT, expected to be dominated by cation—polymer interactions. Using a combination of molecular dynamics simulations and X-ray fluorescence, we show how different anions effectively tune the coordination and chelation of cations by p(g2T-TT). At the same time, softer and hydrophobic anions such as TFSI— and ClO₄— are



found to preferentially interact with the p(g2T-TT) phase, further enhancing the polymer—cation chelation. We highlight how the stronger hydrophobic nature of TFSI⁻ causes its preferential accumulation at the polymer interface, further enhancing the anion-enabled cation—polymer chelation. Besides opening the way for a full study of electrolyte doping mechanisms in operating devices, our results suggest that tailoring the electrolyte for different applications and materials might be a viable strategy to tune the performance of mixed conducting devices.

■ INTRODUCTION

Organic electrochemical transistors (OECTs) are ionic-to-electronic transducers that rely on the ability of the organic active layer to transport both ions and electrons. These devices consist of an electrolyte in direct contact with a π -conjugated polymer channel. Upon an applied voltage, ions driven inside the polymer film induce and compensate excess mobile electronic charge density on the polymer backbone (electrochemical doping). The great interest in OECTs and, more broadly, in mixed transport is proportional to the variety of applications where these devices have disrupted the state-of-the-art: from bioelectronics and healthcare (neural interfaces, chemical and biological sensors to energy production and storage, to artificial synapses. These applications exploit the similarity between OECT operation and the way cells send and receive signals, opening facile integration with biological substrates.

At the heart of OECTs working principle is the active material, which is usually a π -conjugated polymer or polymer blend able to host or be chemically linked to charged groups. The greatest challenges of developing organic mixed ionic-electronic conductors (OMIECs) are the need to optimize the seemingly contrasting processes of electronic and ionic charge transport. In recent years, the strategy of swapping the solubilizing alkyl chains of π -conjugated polythiophenes in

favor of ethylene glycol (EG) side chains has proven a promising strategy to achieve a balance between water permeability, ion mobility, and hole transport efficiency. Among these glycolated mixed conductors, p(g2T-TT) (Figure 1a) demonstrated the best overall figure of merit, 11 achieving high currents at submillisecond time scales, high transconductance, and steep subthreshold switching. 12,13

However, despite the increasing library of OMIECs being tested in devices, comprehensive relationships between chemical modification, molecular and nanoscale morphology, extent of ion penetration, and its impact on device characteristics are still largely missing. For this reason, a few studies aimed at elucidating the mechanism of ion conduction and ion uptake in hydrated p(g2T-TT) films, 14,15 as well as other glycolated polythiophenes, $^{16-18}$ have been carried out. It has been observed that the polymer undergoes swelling when in contact with the electrolyte solution (passive uptake) and again when bias is applied (active uptake). Swelling was found to

Received: May 11, 2020 Revised: August 4, 2020 Published: August 4, 2020





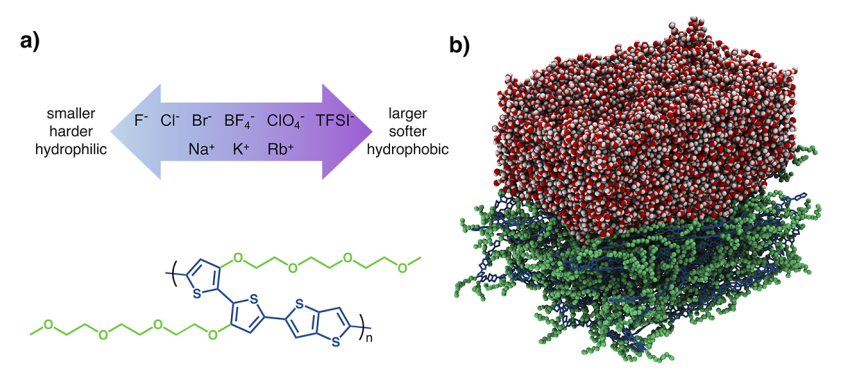


Figure 1. (a) Scheme showing the anions and cations studied in this work as a function of their characteristics, as well as the chemical structure of p(g2T-TT). (b) Details of the simulated interface between p(g2T-TT) and water. Side chains are shown as green spheres while the oligomer backbone is shown as blue lines. 3D periodic boundary conditions apply.

depend on the ion size and the nature of the electrolyte; however, the mass uptake from passive swelling remains around 10% for p(g2T-TT) (unlike for PEDOT/PSS where it can exceed 100%). It appears that the changes in $\pi-\pi$ stacking and lamellar spacing upon doping are irreversible, and the film microstructure is altered after the first doping cycle. This however does not affect the performance, and the device operation is stable. This information suggests that some of the ions could be responsible for this "structural doping" and might be strongly interacting with the EG side chains. 14

It should be noted that such systems likely exhibit a low degree of crystallinity, and because it has been shown that the presence of disordered domains is crucial for ion mobility, the available structural data do not provide a complete picture of how ions interact with p(g2T-TT). Notably, swelling and ion uptake measurements of thin films can only offer an average estimate because water penetration and swelling are expected to be strongly dependent on the local environment in a material characterized by a rich microstructure. For this reason, molecular dynamics (MD) simulations can prove a valuable tool to zoom in at the molecular-scale and probe, separately, polymer—electrolyte interfaces with different degrees of order.

Perhaps one of the crucial understudied aspects regarding the microscopic behavior of OMIECs in devices is how the concentration and nature of the electrolyte affects OECT response and ultimately drives changes in the polymer microstructure. It is understood that during passive swelling (by net-neutral electrolyte), cations interact with the polymer side chains, while upon doping the excess anions penetrating the polymer microstructure are expected to be more closely interacting with the polymer backbone, stabilizing polarons. In this respect, studies relating ion concentration, size, and water uptake to the polymer morphology and performance have recently been reported; 14,17,22,23 however, only very few electrolytes have been investigated.

In this study, we use MD simulations and X-ray fluorescence (XRF) spectroscopy to study p(g2T-TT)—electrolyte interfaces and obtain atomistic insight into polymer—electrolyte interactions. We explore the effect of various salts on the polymer—electrolyte interface as we move along the Hofmeister series: ²⁴ the different cation and anion pairings cover a wide span of ionic radii, charge densities, and hydration properties. In particular, we examine various negative ions ranging from fluoride to ionic liquid species such as bis(trifluoromethylsulfonyl)imide (TFSI). ²⁵ Our study shows

how different anions compete with the EG side chains for cation coordination, with increasingly hydrophobic anions affecting not only cation solubility but also the interfacial properties of p(g2T-TT). These findings can be extended to the general class of π -conjugated polymers with EG side chains.

Our simulations are performed in neutral conditions that mimic the "off" state of an OECT, which undergoes passive swelling and electrolyte uptake. Our study is focused on the interfacial interactions between a pure polymer phase and an electrolyte phase; we have not attempted here to simulate the entire swelling process because, as we stated above, it is not straightforward to estimate the degree of swelling in polymer regions having different microstructures. Furthermore, the microsecond time scale accessible within classical MD simulations is not sufficient to observe polymer swelling. In general, our work is a necessary step toward the simulation of operando conditions, which would involve the presence of excess charges on the polymer backbone and an excess of anions and further insight into the mutual interaction between them. A full description of the interaction between electronic and ionic charge carriers in a realistic environment is however beyond the current state of the art.

In the following three sections, we present results arising from our computational study of the p(g2T-TT)—water interface. We initially focus on the trends in cation—polymer coordination in different electrolytes as a function of their ionic radius, hydration sphere, and water structuring properties. We then analyze the differences in polymer—water hydrogen bonds and polymer surface area as a function of the electrolyte. Next, we show the density and electrostatic potential profiles of the polymer—electrolyte interface, focusing on interactions between hydrophobic anions and p(g2T-TT). In the fourth section, we discuss the XRF study of p(g2T-TT) thin films soaked in various electrolytes; these measurements are interpreted using insight from the MD simulations, providing validation of the anion-enabled chelation observed in silico.

■ RESULTS AND DISCUSSION

A planar interface between p(g2T-TT), water, and various electrolytes (see Figure 1a) was built by interfacing a previously equilibrated bulk p(g2T-TT) periodic box and a water—electrolyte box along the z-axis of the simulation cell (see Computational Methods and Figure S1 for details). The polymer layer was obtained by annealing and equilibrating 20 coiled oligomer bundles made of 16 repeating units each, to

form a compact 2D film characterized by having the conjugated backbone π -stacking roughly parallel to the film plane, which could be described as an edge-on orientation, reflecting the experimentally determined thin-film texture. This entails that most of the solvent-exposed surface area is formed by side chains, while the backbone is largely buried inside the film (see Figures 1b, S1 and Computational Methods). 3D periodic boundary conditions apply, with the water—polymer interface along the z-axis, and the pure polymer/pure water phases continuous along x and y. All electrolytes were added in 1 M concentration. In the case of RbClO₄, the formation of ionic clusters was observed during simulations carried out at 1 M concentration. This phenomenon has been previously observed for ClO₄ salts. To prevent this, the simulation was carried out in 0.5 M RbClO₄, where the formation of clusters was not observed.

Coordination and Chelation of Cations by p(g2T-TT) Side Chains. In this section, we analyze how water and p(g2T-TT) compete for the coordination environment of Na^+ , K^+ , and Rb^+ ; we then investigate how the nature of the counterion modulates these interactions. Figure 2 shows the

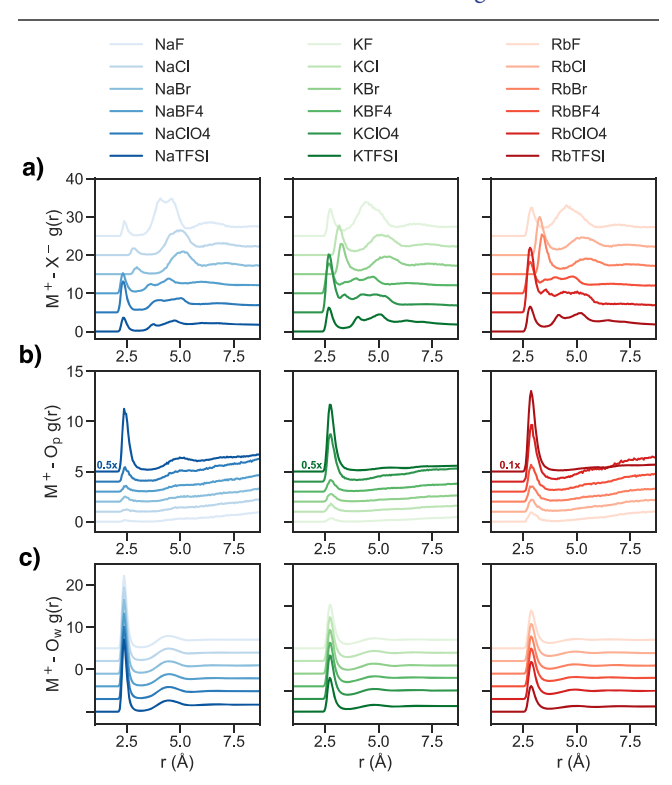


Figure 2. RDF g(r) between $M^+ = Na^+$, K^+ , and Rb^+ and (a) their negative counterions ($X^- = F^-$, Cl^- , Br^- , BF_4^- , ClO_4^- , $TFSI^-$), (b) EG side-chain oxygens O_p and (c) water oxygens O_w . Curves have been vertically shifted for clarity [by 5, 1, and 2.5 Å in panels (a–c), respectively].

radial distribution function (RDF) of each metal cation with respect to its counterion, EG oxygens, and water. As expected, for increasingly larger alkali metals, cation—anion interactions start to dominate the first solvation shell. In the same way, the outer solvation shell is increasingly less structured for heavier cations, whose influence on the water ordering does not extend beyond the first solvation layer. The same effect is seen when swapping harder anions for larger, more hydrophobic ones: BF_4^- , ClO_4^- , and $CFSI^-$ can penetrate the first solvation shell

of Na^+ more effectively than halogens. Interestingly, TFSI-salts show lower RDF peaks with respect to other polyatomic anions (Figure 2a). These changes are accompanied by an increase in the cation—p(g2T-TT) peaks, denoting cation coordination to EG side chains at the expense of water which becomes less tightly bound; this is particularly evident if TFSI- is used as a counterion (Figure 2b). Overall, both the size/hardness of anions and cations play a role in tuning the extent of cation—polymer interactions.

We then took a closer look at the cation—polymer interactions, quantifying the fraction of cations coordinated to at least one oxygen from the p(g2T-TT) side chains for any given MD snapshot (Figure 3a). The probability jumps by over 1 order of magnitude when swapping a halogen salt with a TFSI⁻ salt. This effect is also amplified by choosing a softer cation: as seen in Figure 2, Na⁺ is significantly less likely to shed water molecules from its coordination shell and allow the glycolated side chains to replace them; K⁺ and Rb⁺ instead show a higher propensity to swap their loosely bound water shell for p(g2T-TT).

In order to distinguish between simple coordination and chelation, we analyzed how many side-chain oxygen atoms were found within a 3 Å radius from each cation. Figure 3b shows how softer counterions not only increase the overall probability of polymer coordination but also promote chelation—defined as coordination by at least two EG oxygens. In the case of Na⁺ salts, chelation is almost absent when harder anions are present; in NaTFSI, it is the prevalent kind of interaction. K⁺ and Rb⁺ salts show chelation even in the presence of fluoride, but the p(g2T-TT) side chains can completely saturate their coordination sphere only if TFSI⁻ is used as the counterion. To conclude, diffuse and larger anions, having less solvating water, can more easily penetrate the first coordination shell of cations; this in turn makes cations available to chelating EG oxygens.

Water-Polymer Hydrogen Bonds and p(g2T-TT) Surface Area. Looking at the hydrogen bonds between the p(g2T-TT) side chains and the solvent can provide us with indirect information on the availability of the side chains at the interface. As expected, the average number of hydrogen bonds is roughly independent of the electrolyte because all simulations have in common the initial polymer conformation (see Figure 4a). However, KTFSI and RbTFSI strongly deviate from the general picture: EG side chains are consistently less available to make hydrogen bonds, which is in line with the stronger chelation tendency discussed previously.

Figure 4b reports the p(g2T-TT) solvent-accessible surface area (SASA) for all studied electrolyte interfaces. Overall, the effect of the electrolyte on the surface area of the polymer appears generally modest, except when TFSI⁻ is present. In the presence of RbTFSI and KTFSI salts, p(g2T-TT) shows markedly higher (SASA) values. This observation, together with the sharp decrease in hydrogen bonds discussed earlier, confirms the increased interaction between the polymer and the electrolyte. We then examined the fraction of surface area corresponding to the EG side-chain oxygen atoms (Figure 4c): the stacked histograms show the separate contributions from oxygens situated at different distances from the polymer backbone. All TFSI- salts show an increase in the exposed oxygen surface area, which concerns all but the oxygen closest to the backbone. These results are in line with the higher hydrophobicity of TFSI⁻, as well as with previous observations concerning the behavior of this and other hydrophobic, larger

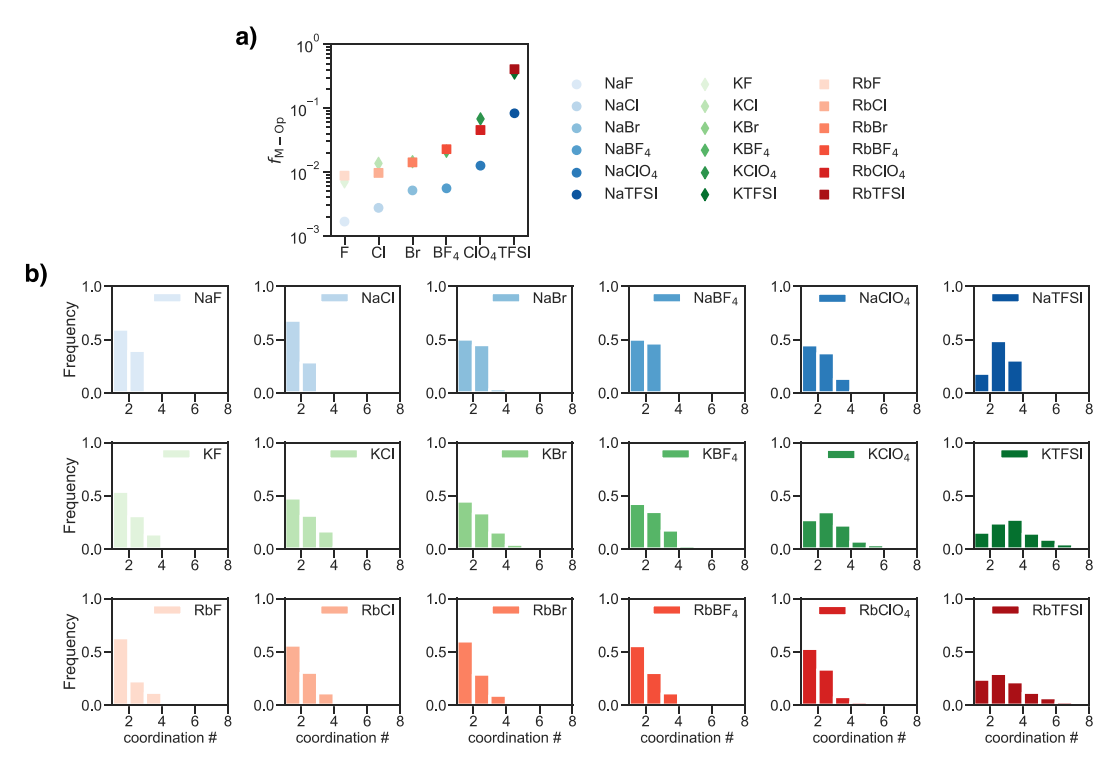


Figure 3. (a) Fraction of alkali cations coordinated to p(g2T-TT), defined as the number of ions having at least one EG oxygen within 3 Å, normalized by the total number of cations in the simulation box over 100 simulation snapshots. (b) Normalized frequency of coordination numbers for alkali ions, defined as the number of oxygen atoms from p(g2T-TT) within a 3 Å radius over 100 simulation snapshots.

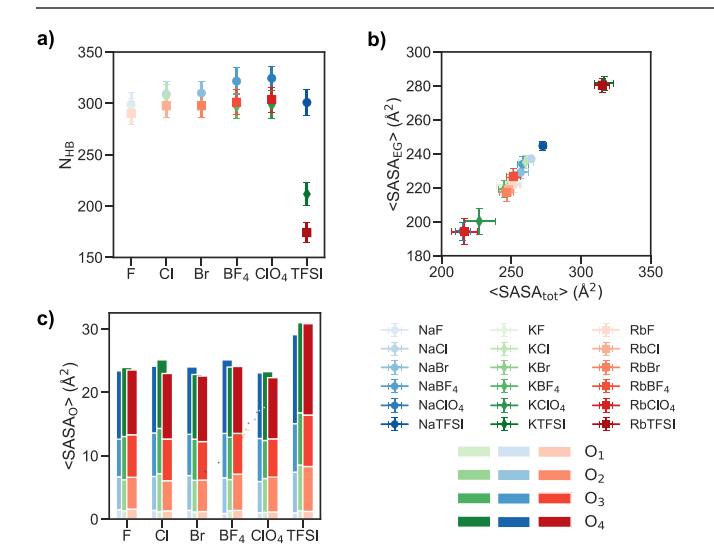


Figure 4. (a) Average number of hydrogen bonds between water and p(g2T-TT). (b) Average solvent accessible surface area, $\langle SASA \rangle$. Blue dots: Na⁺ salts; green diamonds: K⁺ salts; red squares: Rb⁺ salts. (c) Breakdown of the contribution to the p(g2T-TT) SASA from sidechain oxygen atoms, $\langle SASA_O \rangle$, where O_1 is the oxygen closest to the backbone and O_4 is the farthest.

ions. 27,28 Interestingly, when p(g2T-TT) is interfaced with NaTFSI salts, it shows only a modest decrease in the number of hydrogen bonds with water with respect to other Na salts, as well as a slightly lower side chain $\langle SASA_O \rangle$ when compared to KTFSI or RbTFSI. This is related to the previously discussed lower coordination tendency of Na to p(g2T-TT) because of a strongly bound hydration shell, showing that harder cations can effectively modulate the anion—polymer interface.

In summary, we have observed how the size and hardness of both cations and anions play a significant role in modulating the interactions between cations and p(g2T-TT). In this context, the strongest effect is seen with TFSI⁻ salts, in which cation—polymer chelation becomes strongly favored. This is not unexpected, given the size and charge density of this polyatomic anion. In the next section, we investigate how different anions directly affect the polymer interface by looking at the density and electrostatic potential profiles.

Density and Electrostatic Potential Profiles at the **Water**-p(g2T-TT) **Interface.** To probe the existence of specific anion-polymer interactions, we calculated the RDF between anions and either EG side-chain oxygens or backbone sulfur atoms (Figure S2). Unlike halogens where no specific interactions or close contacts are present, larger anions such as BF₄-, ClO₄-, and TFSI- show a higher affinity with the polymer. The EG side-chain-anion RDF increases with increasing cation coordination, with peaks around 5 Å. For KTFSI and RbTFSI, this RDF peak is almost unity; this result is consistent with the highest (SASA_O) calculated for these systems (Figure S2a). In the case of ClO₄ and TFSI, the two most hydrophobic ions studied, the RDFs show the presence of close contacts with the exposed polymer backbone (Figure S2b). These are accompanied by corresponding peaks in the cation-sulfur RDF (Figure S2c).

We then calculated the electrostatic potential profile across the simulation box, as shown in Figures 5a and S4. The drop from higher to lower potential is identifiable as the interface region between p(g2T-TT) and water. The lower contrast between the two phases is observed both with softer cations (i.e., KF and RbF vs NaF) and with larger anions, particularly TFSI⁻. The density profiles of all electrolytes and p(g2T-TT) in Figure 5b reveal how TFSI⁻ tends to concentrate at the water—p(g2T-TT) interface. This is seen also for ClO₄ salts,

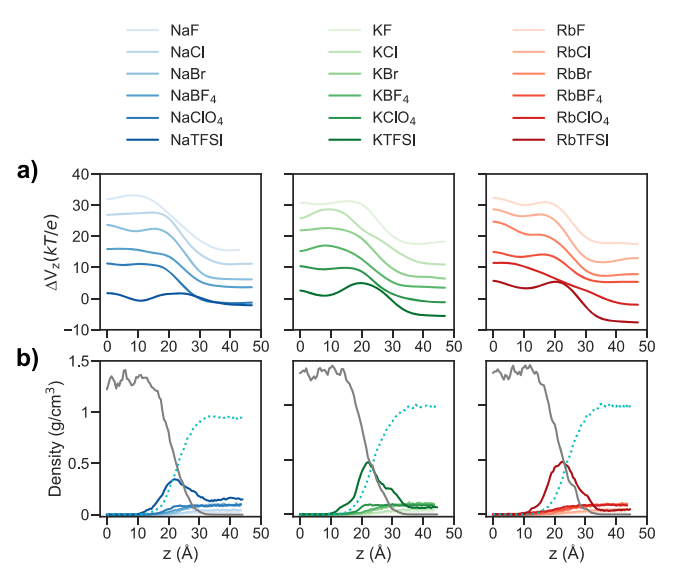


Figure 5. (a) Change in electrostatic potential ΔV along the vertical axis z. Curves have been vertically spaced by 5 kT/e for clarity. (b) Density profile along the z-axis of p(g2T-TT) (gray line), water (cyan dots), and anions (color gradient solid lines). Both electrostatic energy and density profiles have been averaged along the z-axis; full profiles are reported in Figures S4 and S5; z=0 corresponds to the middle of the p(g2T-TT) phase.

albeit to a lower extent (see also Figure S5). Interestingly, while with Rb⁺ and K⁺ the concentration of TFSI⁻ is highest at the polymer interface, the presence of Na increases the solubility of TFSI⁻ in water, as seen from the higher density in the water phase. This observation also matches the lowest drop in electrostatic potential seen for NaTFSI. Overall, the different behaviors of TFSI⁻ and ClO₄⁻ can be explained considering the higher hydrophobicity of these anions. A closer look at the polymer—electrolyte close contacts for KTFSI and RbTFSI is shown in Figure S6.

In summary, our MD simulations showed the importance of different anions in the modulation of polymer—electrolyte interactions. The use of large and softer anions not only enhances cation—polymer chelation but in some cases also results in a modification of the polymer—water interface because of the marked hydrophobic character of species such as TFSI. In the next section, we discuss the experimental validation of these results carried out via XRF for a series of TFSI salts, with the aim of quantifying the TFSI—polymer interactions and TFSI-enhanced cation chelation.

XRF Study of OECTs with Rb and K Salts. Quantifying the ion-p(g2T-TT) interactions in electrolyte-infiltrated OMIECs presents a difficult experimental task. X-ray techniques provide one route to probe ion composition and local ion environment. Therefore, ex situ XRF and absorption measurements were carried out on electrolyte-exposed films of p(g2T-TT). Care was taken to use neutral electrolytes (pH \sim 6-8). XRF was carried out on neat films and films exposed to K⁺- and Rb⁺-based electrolytes, as shown in Figure 6 (the Na⁺ K_{α} peak energy of 1.04 keV was outside the energy range of the experimental apparatus, thus Na-based salts where excluded). The TFSI⁻ induced cation—polymer chelation was measurable as an increase in XRF as more cations were expected to be entrained in TFSI-based electrolyte exposed films of p(g2T-TT), as compared to those exposed to metal-halogen electrolytes. Films of p(g2T-TT) ex situ exposed to 1 M

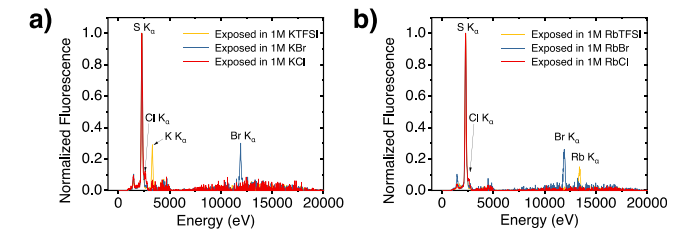


Figure 6. XRF spectra of p(g2T-TT) films ex situ exposed to 1 M aqueous solutions of (a) KTFSI, KBr, and KCl and (b) RbTFSI, RbBr, and RbCl, each normalized to S K_{α} fluorescence. Individual XRF spectra are reported in Figure S7.

aqueous KCl, KBr, RbCl, and RbBr showed no evidence of retained cations (i.e., absence of resolvable K or Rb K_{α} peaks). Accounting for the noise floor of the X-ray detector, in the case of Rb⁺ this would imply a cation concentration of at most 0.005 cations per heterocyclic sulfur. Conversely, films of p(g2T-TT) ex situ exposed to 1 M aqueous KTFSI and RbTFSI showed clear K and Rb K_{α} peaks, respectively, which matches the predicted anion-enabled chelation.

While the simulations do not account for charge on the polymer backbone, it is expected that p(g2T-TT) processed in ambient be oxidized to some degree. 29 This is manifest in the XRF spectra of films exposed to KCl, KBr, RbCl, and RbBr which, while showing no measurable cation fluorescence, displayed fluorescence from anions (Cl⁻ or Br⁻) presumably balancing positive charge on the partially oxidized p(g2T-TT). Similarly, the S K_{α} peak increased following exposure to KTFSI and RbTFSI. Because of the large separation in energies of S, Br, and Rb K_{α} peaks, these presented an ideal case to convert the qualitative spectral change to quantitative anion and cation compositional changes. Subtracting the XRF spectra collected before and after electrolyte exposure revealed a consistent 15-17% increase in S fluorescence, representing an entrained anion concentration of 1 TFSI⁻ per ~12.5 heterocyclic sulfurs or 1 TFSI⁻ per ~3 repeat units. Known S, Br, and Rb composition samples were prepared and measured with XRF to produce compositional calibration curves. Samples exposed to KBr and RbBr displayed an uptake of 0.047 and 0.048 Br per heterocyclic sulfur, respectively. This translates to around one Br every five repeat units for both KBr and RbBr exposed films. As mentioned above, this Br is presumed to be balancing positive charge on the partially oxidized p(g2T-TT).

Samples exposed to RbTFSI displayed an uptake of 0.051 Rb⁺ ions per heterocyclic sulfur and 0.079 TFSI⁻ per heterocyclic sulfur. The excess TFSI⁻ is consistent with the halogen-anion concentration present to counterbalance the positive charge on p(g2T-TT) because of its partially oxidized state. The oxidation of the polymer cannot explain the preferential uptake of Rb⁺ when the TFSI⁻ anion is employed because both RbTFSI and RbBr show a similar anion uptake because of the partial p(g2T-TT) oxidation. Thus, it seems highly likely that the presence of Rb⁺ cations is due to the predicted TFSI⁻-enabled cation-side-chain chelation. KCl, KBr, and KTFSI followed the same qualitative trends. The TFSI⁻-enabled cation-side-chain chelation was observed to be reversible with no cation or anion XRF signal present after multiple soak and rinse cycles with deionized (DI) water.

Extended X-ray absorption fine structure (EXAFS) was carried out on p(g2T-TT) films exposed to Rb^+ -based electrolytes. The high level of disorder, relative long length scales, and difficulties with contrast undermined the effective-

ness of ex situ EXAFS. Ambient EXAFS at the Rb⁺ K edge lacked the resolution to confirm RDFs or discern changes in the Rb environment because of the anion choice.

CONCLUSIONS

In summary, we have carried out both XRF and MD simulations on a series of p(g2T-TT)—electrolyte interfaces. We have analyzed the effect of different counterions on the p(g2T-TT)—water interface and their ability to modulate coordination and chelation of metal cations. We have shown how softer polyatomic anions, particularly TFSI⁻ and ClO₄⁻, can enhance cation coordination and chelation by EG side chains. The higher hydrophobic character of TFSI⁻ results in a tendency to concentrate at the p(g2T-TT) interface, increasing both the surface area of the polymer and the cation-side-chain chelation. On the other hand, the use of smaller, harder cations such as Na⁺ can mitigate this effect by increasing the solubility of TFSI in water. These trends are consistent with the literature on PEO—water interfaces, 30-33 and they may translate in significant differences in the context of operating OFCT:

Our results can be directly compared to a working OECT in the "off" state undergoing passive uptake. The trends observed in this work open new discussions and speculations on how the choice of the electrolyte might affect the device morphology and OECT operation, not only in the specific case of p(g2T-TT) but also for the general family of glycolated polymers. Overall, our data fits within existing reports, highlighting how electrolytes can control swelling and modify the polymer microstructure. In this respect, different electrolytes could affect not only doping/dedoping kinetics34,35 but also electronic mobility, 17 suggesting that the choice of the electrolyte should be an important parameter when testing OECTs. These findings are expected to be particularly relevant for applications such as neuromorphic devices, batteries, or supercapacitors that do not involve biological substrates, where strict boundaries of pH and biocompatibility do not apply.

Finally, we highlight the importance of theory and simulations in investigating the dynamics and structure of mixed transport materials. MD simulations, coupled with ab initio or semiempirical methods aimed at capturing polarization effects on the polymer electronic structure, will prove a robust tool to gain a general understanding of OMIECs and develop a theory of mixed transport able to guide the rational design of polymer mixed conductors. In this context, the simulations performed in this work will be the basis of further investigations on the doping kinetics of p(g2T-TT), for which a rigorous theoretical model is still lacking.

■ COMPUTATIONAL METHODS

Force Field and Software Details. The general amber force field 2 (GAFF2)³⁶ for p(g2T-TT) was reparameterized for the g2T-TT repeating unit, with RESP partial charges obtained at B3LYP/6-31G* level. The torsional parameters for dihedrals between aromatic units were obtained from fitting B3LYP/6-31G*/MP2 potential energy surface scans. DFT and MP2 calculations were performed using GAMESS-US³⁷ and ORCA.³⁸ The water model SPC/E³⁹ was chosen because of its proven reliability in high ionic strength environments.⁴⁰ Force field parameters for BF₄⁴¹ and TFSI⁴² ions were taken from Agilio Padua's GitHub repository; ⁴³ those for ClO₄⁴⁴ were taken from Bryce's Amber parameter database.⁴⁵ The systems were prepared using PACKMOL⁴⁶ and antechamber.⁴⁷ MD simulations were performed using Amber16.⁴⁸ The postproduction analysis was

performed using in-house Python code based on the MDAnalysis library. 49,50 Electrostatic potential maps were obtained using VMD. 51

System Setup. A total of 20 polymer chains of 16 repeating units were simulated. The polymer film was built by merging two preannealed polymer bundles containing 10 chains each and annealing the system under 3D periodic boundary conditions at 500 K until a stationary density was achieved. A layer of SPC/E water was then added to simulate a planar interface and the system was reequilibrated at 298.15 K for 100 ns. Finally, different alkali salts (cations: Na⁺, K⁺, Rb⁺; anions: F⁻, Cl⁻, Br⁻, BF₄⁻, ClO₄⁻, TFSI⁻) in 1 M concentration (0.5 M for RbClO₄) were added to the preequilibrated interfaces, and the resulting system was simulated for an additional 600 ns. The 20 polymer chains consisting of 16 repeating units each are oriented with the backbone parallel to the y-axis; the water—polymer interface is along the z-axis.

EXPERIMENTAL MATERIALS AND METHODS

Potassium chloride (>99.0%), potassium bromide (>99.0%), potassium carbonate (99.8%), and rubidium carbonate (99.8%) were purchased from Sigma-Aldrich; bis(trifluoromethane)-sulfonimide (>99.0%) was purchased from TCI America; rubidum chloride (99.8%) and rubidium bromide (99.8%) were purchased from Alfa Aesar. Potassium bis(trifluoromethane)sulfonimide ad rubidium bis(trifluoromethane)sulfonimide were synthesized following a modified previously published method. Poly(2-(3,3'-bis(2-(2-methoxyethoxy)ethoxy)ethoxy)-[2,2'-bithiophen]-5-yl)thieno[3,2-b]thiophene) was synthesized following previously published methods.

Thin films samples of p(2T-TT) were drop-cast in a saturated chloroform environment on 25 μm polyimide films from 5 mg/mL solutions in chloroform. Prior to drop-casting, polyimide films were sonicated in acetone and isopropyl alcohol followed by a 10 min UV—ozone exposure. Prior to electrolyte exposure, films were soaked and rinsed with DI water several times to remove any metal-halide impurities. Ex situ electrolyte exposure was performed by immersing the thin film samples in 1 M aqueous salt solutions for 30 min. Following exposure, thin film samples were quickly rinsed with DI water to displace the liquid electrolyte form the surface and blown dry with nitrogen flow.

XRF spectra were collected with a Xenemetrix ED-XRF-measure unit with a rhodium white light X-ray source. The energy range was set at 20 keV. In order to improve the signal-to-background ratio for light elements including S, Cl, and K, a titanium filter was placed between the X-ray source and the sample to remove the Rh L lines. The measurement was carried out under vacuum with 300 s exposures. For the data analysis, peaks were simulated by single Gaussian peaks to quantify their positions and areas. A calibration curve was constructed by measuring a series of known composition mixtures of thiourea and rubidium salts spin-coated on 25 μm polyimide films. EXAFS was carried out on the bending magnet beamline in Sector 5 (DND-CAT) of the Advanced Photon Source at Argonne National Laboratory.

ASSOCIATED CONTENT

5 Supporting Information

The Supporting Information is available free of charge at https://pubs.acs.org/doi/10.1021/acs.chemmater.0c01984.

Additional analysis of MD simulations, individual XRF spectra, synthetic details, and NMR spectra (PDF)

AUTHOR INFORMATION

Corresponding Author

Micaela Matta — Department of Chemistry, Northwestern University, Evanston, Illinois 60208, United States; Department of Chemistry, University of Liverpool, Liverpool L69 7ZD, U.K.; oorcid.org/0000-0002-9852-3154;

Authors

- Ruiheng Wu Department of Biomedical Engineering, Northwestern University, Evanston, Illinois 60208, United States
- Bryan D. Paulsen Department of Biomedical Engineering, Northwestern University, Evanston, Illinois 60208, United States
- **Anthony J. Petty, II** Department of Biomedical Engineering, Northwestern University, Evanston, Illinois 60208, United States
- Rajendar Sheelamanthula KAUST Solar Center (KSC), King Abdullah University of Science and Technology (KAUST), Thuwal 23955-6900, Saudi Arabia
- Iain McCulloch KAUST Solar Center (KSC), King Abdullah University of Science and Technology (KAUST), Thuwal 23955-6900, Saudi Arabia; Department of Chemistry and Center for Plastic Electronics, Imperial College London, London W12 0BZ, U.K.
- George C. Schatz Department of Chemistry, Northwestern University, Evanston, Illinois 60208, United States; orcid.org/0000-0001-5837-4740
- Jonathan Rivnay Department of Biomedical Engineering, Northwestern University, Evanston, Illinois 60208, United States; Ocid.org/0000-0002-0602-6485

Complete contact information is available at: https://pubs.acs.org/10.1021/acs.chemmater.0c01984

Author Contributions

M.M. performed the simulations, analyzed the results, and drafted the manuscript. M.M., R.W., B.D.P., and J.R. conceived the experiments. R.W. and B.D.P. carried out the experiments and analyzed the results. A.J.P. and R.S. synthesized and characterized the TFSI salts and conjugated polymer, respectively. All authors contributed to the writing of the manuscript.

Funding

M.M. and G.C.S. were supported by NSF grant CMMI-1848613. RW, BDP, and J.R. gratefully acknowledge support from the National Science Foundation grant no. NSF DMR-1751308. This work used the Extreme Science and Engineering Discovery Environment (XSEDE) BRIDGES at the Pittsburgh Supercomputing Center (PSC) through allocation CHE190029. This work made use of the IMSERC at Northwestern University, which has received support from the Soft and Hybrid Nanotechnology Experimental (SHyNE) Resource (NSF ECCS-1542205), the State of Illinois, and the International Institute for Nanotechnology (IIN). Portions of this work were performed at the DuPont-Northwestern-Dow Collaborative Access Team (DND-CAT) located at Sector 5 of the Advanced Photon Source (APS). DND-CAT is supported by Northwestern University, The Dow Chemical Company, and DuPont de Nemours, Inc. This research used resources of the Advanced Photon Source, a U.S. Department of Energy (DOE) Office of Science User Facility operated for the DOE Office of Science by Argonne National Laboratory under contract no. DE-AC02-06CH11357.

Notes

The authors declare no competing financial interest.

ACKNOWLEDGMENTS

M.M. is grateful to Prof. Alessandro Troisi for useful comments during the preparation of this manuscript. R.W. and B.D.P. are grateful to Dr. Christos D. Malliakas for helpful discussion.

REFERENCES

- (1) Rivnay, J.; Inal, S.; Salleo, A.; Owens, R. M.; Berggren, M.; Malliaras, G. G. Organic Electrochemical Transistors. *Nat. Rev. Mater.* **2018**, *3*, 17086.
- (2) Inal, S.; Rivnay, J.; Suiu, A.-O.; Malliaras, G. G.; McCulloch, I. Conjugated Polymers in Bioelectronics. *Acc. Chem. Res.* **2018**, *51*, 1368.
- (3) Someya, T.; Bao, Z.; Malliaras, G. G. The Rise of Plastic Bioelectronics. *Nature* **2016**, *540*, *379*–*385*.
- (4) Picca, R. A.; Manoli, K.; Macchia, E.; Sarcina, L.; Di Franco, C.; Cioffi, N.; Blasi, D.; Österbacka, R.; Torricelli, F.; Scamarcio, G.; et al. Ultimately Sensitive Organic Bioelectronic Transistor Sensors by Materials and Device Structure Design. *Adv. Funct. Mater.* **2020**, *30*, 1904513
- (5) Scheiblin, G.; Coppard, R.; Owens, R. M.; Mailley, P.; Malliaras, G. G. Referenceless PH Sensor Using Organic Electrochemical Transistors. *Adv. Mater. Technol.* **2017**, *2*, 1600141.
- (6) Mitraka, E.; Gryszel, M.; Vagin, M.; Jafari, M. J.; Singh, A.; Warczak, M.; Mitrakas, M.; Berggren, M.; Ederth, T.; Zozoulenko, I.; et al. Electrocatalytic Production of Hydrogen Peroxide with Poly(3,4-Ethylenedioxythiophene) Electrodes. *Adv. Sustainable Syst.* **2019**, *3*, 1800110.
- (7) Moia, D.; Giovannitti, A.; Szumska, A. A.; Maria, I. P.; Rezasoltani, E.; Sachs, M.; Schnurr, M.; Barnes, P. R. F.; McCulloch, I.; Nelson, J. Design and Evaluation of Conjugated Polymers with Polar Side Chains as Electrode Materials for Electrochemical Energy Storage in Aqueous Electrolytes. *Energy Environ. Sci.* **2019**, *12*, 1349–1357.
- (8) Van De Burgt, Y.; Melianas, A.; Keene, S. T.; Malliaras, G.; Salleo, A. Organic Electronics for Neuromorphic Computing. *Nat. Electron.* **2018**, *1*, 386–397.
- (9) Ling, H.; Koutsouras, D. A.; Kazemzadeh, S.; van de Burgt, Y.; Yan, F.; Gkoupidenis, P. Electrolyte-Gated Transistors for Synaptic Electronics, Neuromorphic Computing, and Adaptable Biointerfacing. *Appl. Phys. Rev.* **2020**, *7*, 011307.
- (10) Paulsen, B. D.; Tybrandt, K.; Stavrinidou, E.; Rivnay, J. Organic Mixed Ionic–Electronic Conductors. *Nat. Mater.* **2020**, *19*, 13–26.
- (11) Inal, S.; Malliaras, G. G.; Rivnay, J. Benchmarking Organic Mixed Conductors for Transistors. *Nat. Commun.* **2017**, *8*, 1767.
- (12) Giovannitti, A.; Sbircea, D.-T.; Inal, S.; Nielsen, C. B.; Bandiello, E.; Hanifi, D. A.; Sessolo, M.; Malliaras, G. G.; McCulloch, I.; Rivnay, J. Controlling the Mode of Operation of Organic Transistors through Side-Chain Engineering. *Proc. Natl. Acad. Sci. U.S.A.* **2016**, *113*, 12017–12022.
- (13) Venkatraman, V.; Friedlein, J. T.; Giovannitti, A.; Maria, I. P.; McCulloch, I.; McLeod, R. R.; Rivnay, J. Subthreshold Operation of Organic Electrochemical Transistors for Biosignal Amplification. *Adv. Sci.* **2018**, *5*, 1800453.
- (14) Cendra, C.; Giovannitti, A.; Savva, A.; Venkatraman, V.; McCulloch, I.; Salleo, A.; Inal, S.; Rivnay, J. Role of the Anion on the Transport and Structure of Organic Mixed Conductors. *Adv. Funct. Mater.* **2019**, 29, 1807034.
- (15) Paterson, A. F.; Faber, H.; Savva, A.; Nikiforidis, G.; Gedda, M.; Hidalgo, T. C.; Chen, X.; McCulloch, I.; Anthopoulos, T. D.; Inal, S. On the Role of Contact Resistance and Electrode Modification in Organic Electrochemical Transistors. *Adv. Mater.* **2019**, *31*, 1902291.
- (16) Bischak, C. G.; Flagg, L. Q.; Yan, K.; Rehman, T.; Davies, D. W.; Quezada, R. J.; Onorato, J. W.; Luscombe, C. K.; Diao, Y.; Li, C.-Z.; et al. A Reversible Structural Phase Transition by Electrochemically-Driven Ion Injection into a Conjugated Polymer. *J. Am. Chem. Soc.* 2020, 142, 7434–7442.

- (17) Flagg, L. Q.; Giridharagopal, R.; Guo, J.; Ginger, D. S. Anion-Dependent Doping and Charge Transport in Organic Electrochemical Transistors. *Chem. Mater.* **2018**, *30*, 5380–5389.
- (18) Flagg, L. Q.; Bischak, C. G.; Quezada, R. J.; Onorato, J. W.; Luscombe, C. K.; Ginger, D. S. P-Type Electrochemical Doping Can Occur by Cation Expulsion in a High-Performing Polymer for Organic Electrochemical Transistors. *ACS Mater. Lett.* **2020**, *2*, 254–260.
- (19) Inal, S.; Rivnay, J.; Hofmann, A. I.; Uguz, I.; Mumtaz, M.; Katsigiannopoulos, D.; Brochon, C.; Cloutet, E.; Hadziioannou, G.; Malliaras, G. G. Organic Electrochemical Transistors Based on PEDOT with Different Anionic Polyelectrolyte Dopants. *J. Polym. Sci., Part B: Polym. Phys.* **2016**, *54*, 147–151.
- (20) Rivnay, J.; Inal, S.; Collins, B. A.; Sessolo, M.; Stavrinidou, E.; Strakosas, X.; Tassone, C.; Delongchamp, D. M.; Malliaras, G. G. Structural Control of Mixed Ionic and Electronic Transport in Conducting Polymers. *Nat. Commun.* **2016**, *7*, 11287.
- (21) Rivnay, J.; Leleux, P.; Ferro, M.; Sessolo, M.; Williamson, A.; Koutsouras, D. A.; Khodagholy, D.; Ramuz, M.; Strakosas, X.; Owens, R. M.; et al. High-Performance Transistors for Bioelectronics through Tuning of Channel Thickness. *Sci. Adv.* **2015**, *1*, No. e1400251.
- (22) Inal, S.; Malliaras, G. G.; Rivnay, J. Optical Study of Electrochromic Moving Fronts for the Investigation of Ion Transport in Conducting Polymers. *J. Mater. Chem. C* **2016**, *4*, 3942–3947.
- (23) Savva, A.; Cendra, C.; Giugni, A.; Torre, B.; Surgailis, J.; Ohayon, D.; Giovannitti, A.; McCulloch, I.; Di Fabrizio, E.; Salleo, A.; et al. Influence of Water on the Performance of Organic Electrochemical Transistors. *Chem. Mater.* **2019**, *31*, 927–937.
- (24) Mazzini, V.; Craig, V. S. J. What Is the Fundamental Ion-Specific Series for Anions and Cations? Ion Specificity in Standard Partial Molar Volumes of Electrolytes and Electrostriction in Water and Non-Aqueous Solvents. *Chem. Sci.* **2017**, *8*, 7052–7065.
- (25) Lee, J.; Kaake, L. G.; Cho, J. H.; Zhu, X.-Y.; Lodge, T. P.; Frisbie, C. D. Ion Gel-Gated Polymer Thin-Film Transistors: Operating Mechanism and Characterization of Gate Dielectric Capacitance, Switching Speed, and Stability. J. Phys. Chem. C 2009, 113, 8972–8981.
- (26) Kim, S.; Kim, H.; Choi, J.-H.; Cho, M. Ion Aggregation in High Salt Solutions: Ion Network versus Ion Cluster. *J. Chem. Phys.* **2014**, *141*, 124510.
- (27) Li, X.; Schatz, G. C.; Nesbitt, D. J. Anion Effects in the Scattering of CO 2 from the Room-Temperature Ionic Liquids [Bmim][BF4] and [Bmim][Tf2N]: Insights from Quantum Mechanics/Molecular Mechanics Trajectories. *J. Phys. Chem. B* **2012**, *116*, 3587–3602.
- (28) Sivan, U. The Inevitable Accumulation of Large Ions and Neutral Molecules near Hydrophobic Surfaces and Small Ions near Hydrophilic Ones. *Curr. Opin. Colloid Interface Sci.* **2016**, 22, 1–7.
- (29) Giovannitti, A.; Rashid, R. B.; Thiburce, Q.; Paulsen, B. D.; Cendra, C.; Thorley, K.; Moia, D.; Mefford, J. T.; Hanifi, D.; Weiyuan, D.; et al. Energetic Control of Redox-Active Polymers toward Safe Organic Bioelectronic Materials. *Adv. Mater.* **2020**, 32, 1908047.
- (30) Su, Y.-l.; Liu, H.-z.; Wang, J.; Chen, J.-y. Study of Salt Effects on the Micellization of PEO-PPO-PEO Block Copolymer in Aqueous Solution by FTIR Spectroscopy. *Langmuir* **2002**, *18*, 865.
- (31) Deyerle, B. A.; Zhang, Y. Effects of Hofmeister Anions on the Aggregation Behavior of PEO-PPO-PEO Triblock Copolymers. *Langmuir* **2011**, *27*, 9203–9210.
- (32) Zajforoushan Moghaddam, S.; Thormann, E. Hofmeister Effect of Salt Mixtures on Thermo-Responsive Poly(Propylene Oxide). *Phys. Chem. Chem. Phys.* **2015**, *17*, 6359–6366.
- (33) Thormann, E. On Understanding of the Hofmeister Effect: How Addition of Salt Alters the Stability of Temperature Responsive Polymers in Aqueous Solutions. *RSC Adv.* **2012**, *2*, 8297.
- (34) Ma, Q.; Zhang, H.; Zhou, C.; Zheng, L.; Cheng, P.; Nie, J.; Feng, W.; Hu, Y.-S.; Li, H.; Huang, X.; et al. Single Lithium-Ion Conducting Polymer Electrolytes Based on a Super-Delocalized Polyanion. *Angew. Chem., Int. Ed.* **2016**, *55*, 2521–2525.

- (35) Schauser, N. S.; Seshadri, R.; Segalman, R. A. Multivalent Ion Conduction in Solid Polymer Systems. *Mol. Syst. Des. Eng.* **2019**, *4*, 263–279.
- (36) Wang, J.; Wolf, R. M.; Caldwell, J. W.; Kollman, P. A.; Case, D. A. Development and Testing of a General Amber Force Field. *J. Comput. Chem.* **2004**, *25*, 1157–1174.
- (37) Schmidt, M. W.; Baldridge, K. K.; Boatz, J. A.; Elbert, S. T.; Gordon, M. S.; Jensen, J. H.; Koseki, S.; Matsunaga, N.; Nguyen, K. A.; Su, S.; et al. General Atomic and Molecular Electronic Structure System. *J. Comput. Chem.* **1993**, *14*, 1347–1363.
- (38) Neese, F. Software Update: The ORCA Program System, Version 4.0. Wiley Interdiscip. Rev.: Comput. Mol. Sci. 2018, 8, No. e1327.
- (39) Berendsen, H. J. C.; Grigera, J. R.; Straatsma, T. P. The Missing Term in Effective Pair Potentials. *J. Phys. Chem.* **1987**, *91*, 6269–6271
- (40) Joung, I. S.; Cheatham, T. E. Molecular Dynamics Simulations of the Dynamic and Energetic Properties of Alkali and Halide Ions Using Water-Model-Specific Ion Parameters. *J. Phys. Chem. B* **2009**, *113*, 13279–13290.
- (41) Lopes, J. N. C.; Deschamps, J.; Pádua, A. A. H. Erratum: Modeling Ionic Liquids Using a Systematic All-Atom Force Field. *J. Phys. Chem. B* **2004**, *108*, 11250.
- (42) Canongia Lopes, J. N.; Pádua, A. A. H.; Shimizu, K. Molecular Force Field for Ionic Liquids IV: Trialkylimidazolium and Alkoxycarbonyl-Imidazolium Cations; Alkylsulfonate and Alkylsulfate Anions. *J. Phys. Chem. B* **2008**, *112*, 5039–5046.
- (43) Padua, A. Force Field for Ionic Liquids https://github.com/agiliopadua/ilff (accessed July 31, 2020).
- (44) Baaden, M.; Berny, F.; Madic, C.; Wipff, G. M3+ Lanthanide Cation Solvation by Acetonitrile: The Role of Cation Size, Counterions, and Polarization Effects Investigated by Molecular Dynamics and Quantum Mechanical Simulations. *J. Phys. Chem. A* **2000**, *104*, 7659–7671.
- (45) Bryce, R. AMBER Parameter Database http://research.bmh. manchester.ac.uk/bryce/amber/ (accessed July 31, 2020).
- (46) Martínez, L.; Andrade, R.; Birgin, E. G.; Martínez, J. M. PACKMOL: A Package for Building Initial Configurations for Molecular Dynamics Simulations. *J. Comput. Chem.* **2009**, 30, 2157–2164.
- (47) Wang, J.; Wang, W.; Kollman, P. A.; Case, D. A. Antechamber, An Accessory Software Package For Molecular Mechanical Calculations. *J. Am. Chem. Soc.* **2001**, 222, U403.
- (48) Case, D. A.; Betz, R. M.; Cerutti, D. S.; Cheatham, T. E.; Darden, T. A.; Duke, R. E.; Giese, T. J.; Gohlke, H.; Goetz, A. W.; Homeyer, N.; et al. *Amber 2016*; University of California: San Francisco, 2016.
- (49) Gowers, R.; Linke, M.; Barnoud, J.; Reddy, T.; Melo, M.; Seyler, S.; Domański, J.; Dotson, D.; Buchoux, S.; Kenney, I.; et al. MDAnalysis: A Python Package for the Rapid Analysis of Molecular Dynamics Simulations. In *Proceedings of the 15th Python in Science Conference*, 2016.
- (50) Michaud-Agrawal, N.; Denning, E. J.; Woolf, T. B.; Beckstein, O. MDAnalysis: A toolkit for the analysis of molecular dynamics simulations. *J. Comput. Chem.* **2011**, *32*, 2319–2327.
- (51) Humphrey, W.; Dalke, A.; Schulten, K. VMD: Visual Molecular Dynamics. *J. Mol. Graphics* **1996**, *14*, 33–38.
- (52) Xue, L.; Padgett, C. W.; DesMarteau, D. D.; Pennington, W. T. Synthesis and Structures of Alkali Metal Salts of Bis-[(Trifluoromethyl)Sulfonyl]Imide. *Solid State Sci.* **2002**, *4*, 1535–1545.